Chinese Chemical Letters 37 (2026) 111159

Contents lists available at ScienceDirect

Chinese Chemical Letters

journal homepage: www.elsevier.com/locate/cclet

Nanothermometry and luminescence modulation *via* separated activators in core-shell-shell fluoride nanoparticles

Bingyu Huang[a], Jipeng Fu[a,*], Tianyi Sun[b], Yuqi Li[b], Jinru Liu[a], Kaina Wang[b], Qian Xu[a], Wengui Yu[a], Hongqi Chen[a], Huajie Luo[b], Mathieu Allix[c], Mingxue Tang[b,*], Shiqing Xu[a,*]

[a] College of Optical and Electronic Technology, China Jiliang University, Hangzhou 310018, China
[b] School of Materials Science and Engineering, University of Science and Technology Beijing, Beijing 100083, China
[c] CNRS, CEMHTI UPR3079, Univ. Orléans, Orléans F-45071, France

ARTICLE INFO

Article history:
Received 19 January 2025
Revised 19 March 2025
Accepted 27 March 2025
Available online 27 March 2025

Keywords:
Core/shell/shell upconversion nanoparticles
Surface phonons
Inert cladding
Nanothermometry
Luminescence modulation

ABSTRACT

Upconversion nanoparticles (UCNPs) have been naturally entangled with surface phonons since their discovery due to their high specific surface area. However, in addition to quenching luminescence at ambient temperatures, surface phonons play a crucial role in activating the dark layer between the sensitizer and the activator to enhance luminescence in thermal environments. Considering that the positive effect of surface phonons may be eliminated under inert cladding, a β-$NaGdF_4$:Yb,Tm@$NaYF_4$@$NaGdF_4$:Yb,Er core-shell-shell upconversion luminescence (UCL) system with two opposite thermo-responsive luminescence behaviors is designed here. The imposition of an inert intermediate shell layer causes the weakening of the blue luminescence of the core Tm ions in the thermal environment, while on the contrary the outermost Er ions realize an effective enhancement of luminescence with the help of surface phonons. In addition, the photoluminescence results show that effective modulation of luminescence color can be achieved by changing the thickness of the inert shell layer, the concentration of Er ions in the activation layer, and the excitation power. Finally, the distinct thermally responsive luminescence behaviors and temperature-dependent color variations enabled moderate temperature sensing and information encryption applications. The maximum relative and absolute sensitivities can be up to 1.62 %/K and 0.64 %/K from 298 K to 573 K, respectively. These findings provided new insights into optimizing the luminescent properties of fluorides and provided a new platform for the application of multiple properties in a material.

© 2026 Published by Elsevier B.V. on behalf of Chinese Chemical Society and Institute of Materia Medica, Chinese Academy of Medical Sciences.

Temperature is a special physical parameter that plays a key role in industrial manufacturing, biomedicine, and fault diagnosis [1–7]. Regarding temperature determination, non-contact upconversion nanoparticles (UCNPs) temperature probes with near-infrared excitation have attracted attention due to their high penetration, sensitivity, and accuracy [8–14]. Specifically, fluorescence intensity ratio (FIR) technology can provide a more efficient temperature response by recording changes in activator emission intensity ratios at different temperatures, which is considered a promising method for temperature measurement [15–19]. Although great effort has been put into exploring high-performance luminescence temperature probes, such as selecting activators with thermally coupled states and mixing the host with two emission centers, achieving high sensitivity that determines temperature resolution remains a daunting challenge [20,21].

The lanthanides (Ln^{3+}) are characterized by an abundance of radiative energy levels and different thermally-dependent electron mobility possibilities, which have invigorated the study of nanoscale temperature probes [22–28]. Usually, it is a popular strategy to use lanthanide ions with thermally coupled energy levels as monitoring targets, such as Er^{3+} ($^2H_{11/2}$ and $^4S_{3/2}$) [29], Ho^{3+} ($^5F_4$ and $^5S_2$) [30] and Tm^{3+} ($^3F_{2,3}$ and $^3H_4$) [31]. Their electron configurations all obey Boltzmann thermal equilibrium allowing enhanced luminescence with increasing temperature, but such neighboring energy states typically have synchronized temperature responses, resulting in lower temperature sensing performance (below 1.0 %/K) and poor signal discrimination [32–34]. In addition to this, another strategy is to mix two materials with different thermally dependent luminescence properties in a certain ratio [35–37]. For example, Martínez *et al.* reported a temperature sensing design that ensembles thermally-quenching large

* Corresponding authors.
E-mail addresses: fujipeng@cjlu.edu.cn (J. Fu), mingxue.tang@hpstar.ac.cn (M. Tang), shiqingxu@cjlu.edu.cn (S. Xu).

https://doi.org/10.1016/j.cclet.2025.111159
1001-8417/© 2026 Published by Elsevier B.V. on behalf of Chinese Chemical Society and Institute of Materia Medica, Chinese Academy of Medical Sciences.

UCNPs (>50 nm) and negatively thermally-quenching small UCNPs (<50 nm), yielding a high sensitivity of 5.88 %/K. However, this strategy depends on the mixing ratio of UCNPs and may increase the likelihood of localized micro-size inhomogeneous distributions, posing a potential problem for accurate sensing. In contrast, combining the non-thermal coupling effects of different lanthanide ions in a single structure to increase S_r by means of a special structural design would be a powerful breakthrough. Another advantage of doing so was to achieve observable thermally responsive luminescent color changes.

The luminescence mechanism that exists between thermally responsive upconversion and the surface environment has recently been explained by surface phonon-assisted energy transfer, clarifying the phonon factors that counteract thermal quenching [38]. More interestingly, core-shell engineering by adding inert or active shells to the core has been developed rapidly, which can avoid the contact of the core ions with the surface quenching and significantly improve the upconversion luminescence efficiency [39–45]. In addition, this design is able to confine the lanthanide luminescent ions to different environments, which provides an effective aid for temperature sensing and color modulation of UCNPs [46]. For example, Yan *et al.* devised a new mechanical design of $LiErF_4$@$LiYF_4$ to achieve ultrasensitive thermally activated upconversion in Er sublattice core-shell nanostructures and exhibit remarkable thermochromic features [47]. Zou *et al.* designed an Ln^{3+}-doped Gd_2O_2S@$NaYF_4$ core/shell heterostructure, which achieved enhanced UCL performance and high relative thermal sensitivity by modulating the interfacial strain by changing the shell composition [48]. All these advances provide power for the design of multifunctional thermally responsive upconversion luminescent materials using upconversion emitters with different luminescent behaviors in the thermal field.

Herein, this work explored the potential of non-thermal coupled energy levels in non-contact nanothermometry and color modulation. A novel $NaGdF_4$:40Yb,1Tm@$NaYF_4$@$NaGdF_4$:20Yb,2Er ($Core_{Tm}$@S_Y@S_{Er}) core-shell-shell UCNPs was proposed to achieve a higher sensitivity of temperature sensing and color modulation by utilizing the thermoresponsive luminescence of the non-thermally coupled energy levels of Tm and Er (Fig. 1a). In addition, the effect of the intermediate inert shell layer on the luminescence intensity and thermoresponsive luminescence behavior of core Tm was systematically investigated and the mechanism present therein was probed. Finally, luminescence color modulation was achieved by introducing different concentrations of Er active shells to compete with the core for photon energy. These results indicated that the luminescence changes induced by the percentage of activator and the different thermoresponsive behaviors with increasing temperature in the core-shell structure had great potential applications in temperature sensing, anti-counterfeiting and information encryption.

Based on an in-depth analysis and study of the nanoscale field, small-sized $NaGdF_4$:40Yb,1Tm ($Core_{Tm}$) and $NaGdF_4$:20Yb,2Er ($Core_{Er}$) UCNPs were synthesized using the reported co-precipitation process (Fig. S1 in Supporting information). In addition to providing the core for the core-shell structure, the different luminescent properties of Tm and Er ions, as illustrated in Fig. 1b, also offered the possibility of realizing the luminescence modulation of the nanomaterials. Based on the hexagonal phase core molding, a modified high-temperature thermal injection process was used to synthesize multilayer core-shell nanoparticles. X-ray powder diffraction (XRD) studies of the synthesized UCNPs at each synthesis step confirmed the successful synthesis of hexagonal-phase multilayered UCNPs (Fig. S2 in Supporting information). Transmission electron microscopy (TEM) micrographs showed the spherical shape of the UCNPs after each synthesis step, and the average diameter increasing from 6.5 ± 0.06 nm in the core to 18.3 ± 0.06 nm in the final multilayered UCNPs (Figs. 1c-g and Fig. S3 in Supporting information). Subsequently, a clear lattice interplanar spacing of 0.521 nm was observed at high resolution, which corresponds to the (100) lattice planes of the $NaGdF_4$ nanocrystals (Fig. 1h).

Small-sized UCNPs are usually limited by severe surface quenching sites, greatly reducing upconversion luminescence intensity and quantum yield. The heterogeneous core-shell structure using the optically inert $NaYF_4$ shell was able to passivate the migration of photon energy to the surface quenching center and change the symmetry of the crystal field around the Tm ions through lattice mismatch, which ultimately increased the probability of radiative relaxation [49]. Therefore, the passivation effect of the inert shell thickness and the luminescence properties on core-shell nanoparticles were investigated here under ambient conditions. As shown in Fig. 2a, the $NaGdF_4$:40Yb1Tm@$NaYF_4$ ($Core_{Tm}$@S_Y) under 980 nm laser excitation exhibited two strong blue band emissions, which can be attributed to the $^1D_2 \rightarrow {}^3H_6$ and $^1G_4 \rightarrow {}^3H_6$ transitions of Tm. As the thickness of the inert shell layer increases steadily from 1 nm to 4 nm, the luminescence intensity of the blue part was enhanced by 20, 197, 409, and 710-fold, which was entirely attributed to the effective elimination of the surface quenching centers by the coating of the inert shell layer. It was worth noting that the increase of shell layer thickness cannot effectively change the luminescence color of core-shell UCNPs, because the inert layer coating makes the enhancement of the blue region significantly higher than that of the UV and red areas. This behavior was demonstrated by the enhancement factor in each luminescence wavelength band (Figs. S4 and S5 in Supporting information). In addition to $NaYF_4$, $NaLuF_4$ and $NaGdF_4$ are often used as inert shell passivationdefects to achieve luminescence enhancement. Here, a comparison was made for different inert shells and the passivation mechanism was explored from the stability point of view through theoretical calculations. The photoluminescence spectra of different shell layers showed that the $NaYF_4$ shell layer was able to realize a significant enhancement of the luminescence effect, which was much higher than that of the $NaLuF_4$ and $NaGdF_4$ shell layers (Fig. S6 in Supporting information). Moreover, the theoretical calculations in Fig. 2b showed the material energy of $NaYF_4$ was much lower than that of Lu and Gd, which suggested that the capping of $NaYF_4$ allowed UCNPs to possess better stability and be beneficial for luminescence applications. Considering that UCNPs have abundant discrete energy levels and possess different heat-dependent electronic transitions, temperature-dependent luminescence studies were performed here on prepared $Core_{Tm}$ UCNPs. Photoluminescence results showed that when the temperature was increased to 573 K, Tm enhanced its luminous intensity by 71-fold in the blue region, 69-fold in the red region, and 147-fold in the entire visible band, which suggested that Core underwent a pronounced negative thermal quenching (Fig. 2c and Fig. S7 in Supporting information). This luminescence enhancement behavior was attributed to the partial chelation of Yb by surface oxygen, *i.e.*, [Yb-O] [38]. Since the surface of the $Core_{Tm}$ UCNPs was covered with carboxyl groups of oleic acid, more surface phonons locally coupled to Yb become more active with increasing temperature. The presence of [Yb-O] and the inclusion of phonon vibrational at multiple frequencies in oleic acid was demonstrated here by Raman spectroscopy and Fourier-transform infrared spectroscopy (FTIR). The peaks at 1454 and 1558 cm^{-1} belong to the asymmetric and symmetric stretching vibrations of COO^- and at 2856 and 2925 cm^{-1} belong to the asymmetric and symmetric stretching vibrations of -CH_2/-CH_3. The wavenumbers of 247, 296 and 355 cm^{-1} originate from the phonon frequencies of the fluoride crystals, while the frequencies of 471, 491, 559 and 620 cm^{-1} are supposed to come from the [Yb/Y/Tm-O] ligand (Figs. S8 and S9 in Supporting information). This [Yb-O] complex can

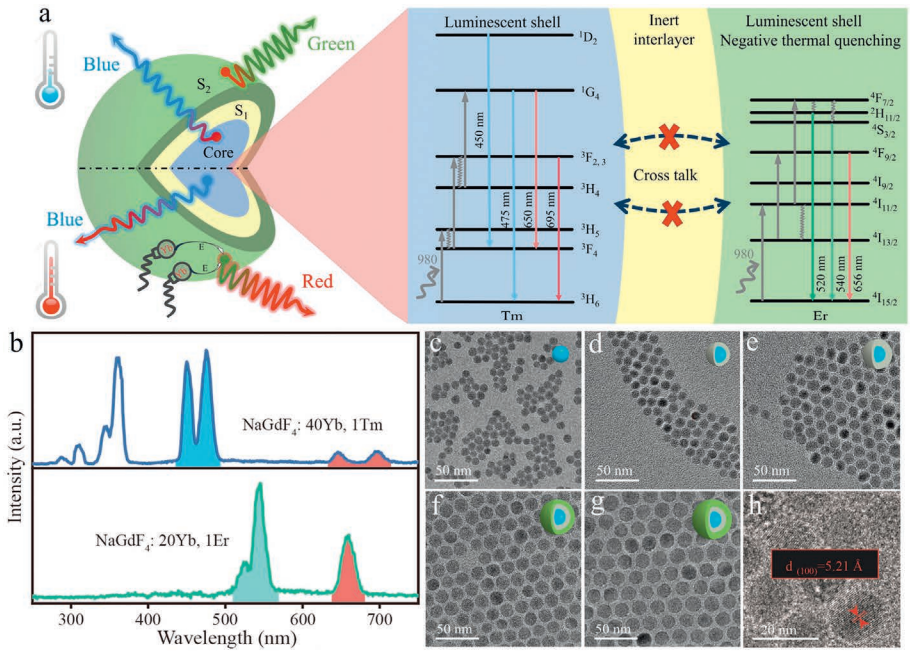


Fig. 1. (a) Schematic representation of $Core_{Tm}@S_Y@S_{Er}$ upconversion nanostructures for color modulation and ratiometric nanothermometry. (b) Upconversion emission spectra of $Core_{Tm}$ and $Core_{Er}$ UCNPs. The spectra were recorded under 980 nm laser irradiation at a pump power of 0.1 W. (c-g) Transmission electron microscopy (TEM) images of the core, different inert shell thicknesses (2 nm and 3 nm) and different active shell thicknesses (2 nm and 3 nm). Scale bar: 50 nm. (h) High-resolution TEM images corresponding to $Core_{Tm}@S_Y@S_{Er}$. Scale bar: 20 nm.

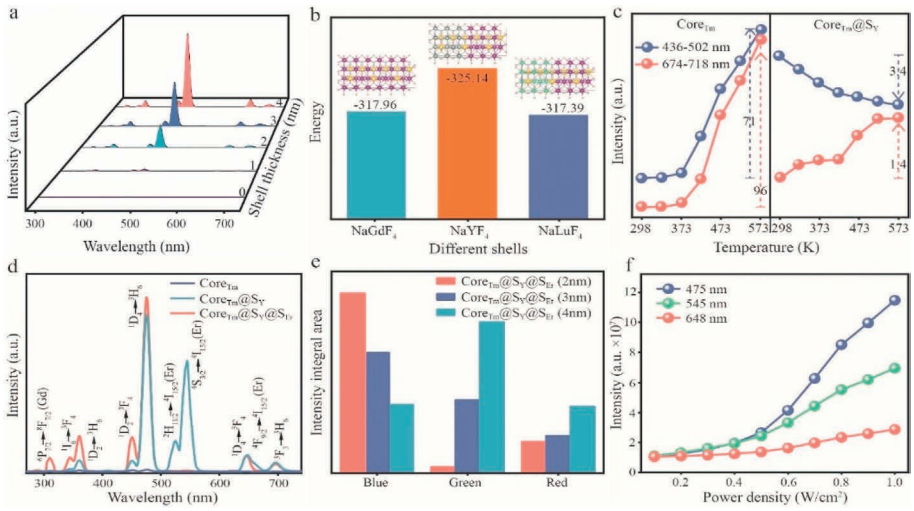


Fig. 2. Optical and thermal response luminescence properties of core and core-shell structures. (a) Upconversion emission spectra of core-shell UCNPs with different inert shell thicknesses (1, 2, 3 and 4 nm). (b) Material energies after cladding the $Core_{Tm}$ using different inert shell layers. The inset represents a schematic diagram of the different core-shell structures. (c) Temperature-dependent upconversion luminescence intensity from 298 K to 573 K at 475 nm and 698 nm for $Core_{Tm}$ and $Core_{Tm}@S_Y$ with an inert shell layer thickness of 2 nm UCNPs. The direction of the arrow indicates an increasing or decreasing trend of luminescence. (d) Upconversion luminescence spectra of $Core_{Tm}$, $Core_{Tm}@S_Y$ and $Core_{Tm}@S_Y@S_{Er}$. The spectra were recorded under 980 nm laser irradiation at a pump power of 0.1 W. (e) Integration of luminescence intensity in the blue, green and red regions with increasing thickness of the $NaGdF_4$:20Yb,2Er shell layer. (f) Relationship between laser excitation power and photoluminescence intensity of prepared $Core_{Tm}@S_Y@S_{Er}$.

also activate the dark layer between the sensitizer Yb to the activator Tm, facilitating energy transfer from Yb to Tm and ultimately producing brighter upconversion emission. Notably, a similar negative thermal quenching effect was observed in $Core_{Er}$ UCNPs (Fig. S10 in Supporting information).

In order to further substantiate the important role of [Yb-O] in generating surface phonons to enhance the upconversion luminescence efficiency in a thermal field, evidence was collected by reverse logic examination of materials without [Yb-O] coordination on the surface. As shown in Fig. 2c, the isolation of [Yb-O] on the surface of $Core_{Tm}$ UCNPs was achieved using $Core_{Tm}@S_Y$ UCNPs encapsulated with a 2 nm $NaYF_4$ inert shell layer (Figs. S11 in Supporting information). This may prevent the molecular assist of the surface oleic acid from acting on the rare earth ions in $Core_{Tm}$, resulting in the loss of the original negative thermal quenching effect of Tm (Figs. S12 and S13 in Supporting information). The temperature-dependent emission spectra of $Core_{Tm}@S_Y$ UCNPs indicated that the presence of the shell layer caused to a 3.4-fold attenuation of the Tm luminescence intensity at 436–502 nm. This result indicated that the encapsulation in the shell layer made the thermally responsive luminescence behavior of $Core_{Tm}$ UCNPs change from negative thermal quenching to thermal quench-

ing, which indirectly proved the importance of [Yb-O] in realizing the thermal enhancement of nanomaterials. In addition, a 1.4-fold enhancement of Tm luminescence at 674–718 nm was observed, which was entirely attributed to the thermal coupling effect.

In order to better achieve the luminescence color modulation and temperature sensing performance, the $NaYF_4$ interlayer with a thickness of 2 nm and the $NaGdF_4$:20Yb, 2Er activation shell were selected here. This strategy can effectively improve the overall luminescence intensity, reduce the energy relaxation between activators and change the luminescence effect of the two activators in the thermal environment. As shown in Fig. 2d, the characteristic peaks of both Tm and Er ions can be observed in $Core_{Tm}@S_Y@S_{Er}$ UCNPs, which clearly indicated that the luminescence combination of the core and shell layers jointly consumes photon energy. The addition of the Er ions contained shell layers caused a significant attenuation of the luminescence of Tm in the core and an obvious change in the overall blue to green ratio of the $Core_{Tm}@S_Y@S_{Er}$ UCNPs, which shifted the luminescence color of the core-shell-shell UCNPs from the blue to the green color gamut (Fig. S14 in Supporting information). This phenomenon may be attributed to the Yb-Er mediated excitation energy depletion in the outer shell layer weakening the absorption of input photon energy by Yb-Tm in the core. To further verify this effect in multilayer systems, $Core_{Tm}@S_Y@S_{Er}$ UCNPs with different thicknesses of $NaGdF_4$:20Yb,2Er shell layers were prepared by increasing the number of thermal injections. The photoluminescence results under 980 nm excitation showed that the blue emission intensity decreased from 106.09 to 39.5, the green emission intensity increased from 3.5 to 91.9, and the red region increased from 18.7 to 39.6 with the increased of the thickness of the $NaGdF_4$:20Yb,2Er shell layer (Fig. 2e and Fig. S15 in Supporting information). This indicated that there was some competition between Yb-Tm in the core and Yb-Er in the shell under the condition of constant laser power. Although Yb in the core can in principle efficiently absorb 980 nm photon energy for Tm upconversion emission, most of the excitation photon energy was absorbed by Yb in the shell layer to enhance Er emission as the thickness of the active shell layer increases. This behavior led to insufficient excitation of Yb in the core and a significant reduction in blue light intensity, so the $Core_{Tm}@S_Y@S_{Er}$ UCNPs with a thick active shell were observed to be significantly green emitting under 980 nm laser pumping. Meanwhile, this also provided some help for multicolor luminescence modulation and luminescence application expansion.

Luminescence is a highly nonlinear process and the excitation irradiance is likely to have different enhancement effects on the luminescence band. The luminescence properties of $Core_{Tm}@S_Y@S_{Er}$ UCNPs under different 980 nm laser power excitations were investigated here. The $Core_{Tm}@S_Y@S_{Er}$ UCNPs showed strong power-dependent upconversion luminescence and a corresponding change in emission color from green to blue as the excitation power was tuned from 0.1 W to 1.0 W (Figs. S16 and S17 in Supporting information). The blue, green and red emission intensities were further plotted as a function of excitation power. As shown in Fig. 2f, the blue luminescence emission was much higher than that of green and red, which can explain the predominantly blue emission of the $Core_{Tm}@S_Y@S_{Er}$ UCNPs under high-power excitation. The combination of the above luminescence behavior of UCNPs at room temperature provided a new idea for achieving accurate luminescence color modulation (Fig. 3a).

$Core_{Tm}@S_Y@S_{Er}$ UCNPs with an active shell thickness of 3 nm and activators located in both environments provided an opportunity to modulate luminescent behavior in thermal environments. The temperature-dependent upconversion emission spectra under 980 nm excitation were plotted in Fig. 3b. The green emission of the shell-most layer Er at 520 and 540 nm ($^2H_{11/2} \rightarrow {}^4I_{15/2}$ and $^4S_{3/2} \rightarrow {}^4I_{15/2}$) progressively enhanced with temperature until 573 K, which was a function of the thermally coupled emission bands [50]. Notably, the most pronounced enhancement of red emission at 658 nm may be attributed to the role of [Yb-O] in facilitating the energy transfer from the sensitizer Yb to the activator Er, which ultimately produced brighter upconversion red emission. In contrast, the blue emission of Tm in the core at 475 and 450 nm decreased weakly with increasing temperature, which may be attributed to the fact that the core was enclosed in the interior without the assisted enhancement of surface phonons. However, an enhancement of Tm emission at 698 nm can still be detected, which was fully attributed to the help of thermal coupling effects.

Based on the different luminescent behaviors of Tm and Er in $Core_{Tm}@S_Y@S_{Er}$ UCNPs under ambient temperature variations, it can be applied to non-contact temperature sensing. Therefore, the fluorescence intensity ratio (FIR) of the two emission bands centered at 475 nm ($I_{Tm\text{-}475}$) to 655 nm ($I_{Er\text{-}655}$) can be well fitted by the following equation:

$$FIR = \frac{I_{Tm-475}}{I_{Er-655}} = y_0 + A\exp^{\frac{R_0}{T}} \quad (1)$$

where y_0, A and R_0 are constants associated with the $Core_{Tm}@S_Y@S_{Er}$ UCNPs system, and T denote the Kelvin temperature. On this basis, the absolute and relative temperature sensitivities (S_a and S_r) were derived and calculated from the following equations [51]:

$$S_a = \left|\frac{\partial FIR}{\partial T}\right| = B\exp(-C/T) \times \frac{C}{T^2} \quad (2)$$

$$S_r = \left|\frac{\partial FIR}{\partial T} \times \frac{1}{FIR}\right| \times 100\% = \frac{B\exp(-C/T)}{B\exp(-C/T) + D} \times \frac{C}{T^2} \times 100\% \quad (3)$$

As the temperature increases from 298 K to 573 K, the integral intensity ratio of 475–655 nm significantly decreased by 13-fold and was well fitted by Eq. 1 (Fig. 3c). Based on these conditions, the maximum S_a and S_r were up to 0.26 %/K and 1.64 %/K from 298 K to 573 K (Fig. 3d). Most temperature sensing used materials containing the thermally coupled energy levels Er^{3+} ($^2H_{11/2}$, $^4S_{3/2}$) and Ho^{3+} ($^5D_0$, $^5S_2/^5F_4$), which leads to inherent drawbacks such as low temperature resolution and insignificant color change with temperature. However, in contrast to other strategies using UV and NIR excitation, the temperature sensing sensitivity of $Core_{Tm}@S_Y@S_{Er}$ UCNPs was measured by integrating wavelengths in the non-thermally coupled bands of the two activators. The use of this non-thermal coupling band provided moderate S_r and S_a, while the significant change in color also conferred self-referencing capabilities, demonstrating the advantages of $Core_{Tm}@S_Y@S_{Er}$ UCNPs designed for nanothermometry (Table S1 in Supporting information).

In order to better elucidate the excellent performance of $Core_{Tm}@S_Y@S_{Er}$ UCNPs with respect to temperature, upconversion luminescence spectra were tested with rapid cycling between high and low temperatures. The temperature-dependent photoluminescence results showed that the $Core_{Tm}@S_Y@S_{Er}$ UCNPs maintained their original brightness and crystal structure integrity after 5 cycles (Fig. 3e and Fig. S18 in Supporting information), which indicated that the UCNPs remained stable and durable up to 573 K. It was worth noting that similar structural stability was observed in $Core_{Tm}$ in thermal environments (Fig. S19 in Supporting information). In addition, the role of temperature variation in modulating the emission color was also verified here. The $Core_{Tm}@S_Y@S_{Er}$ UCNPs produced blue and green pooled emissions at room temperature, and the intensity of the luminescence in blue and green varied weakly with increasing temperature. In contrast, the emission at 655 and 695 nm showed a significant negative thermal quenching, which shifted the overall color of the material towards the red color gamut (Fig. 3f). Based on these properties, $Core_{Tm}@S_Y@S_{Er}$

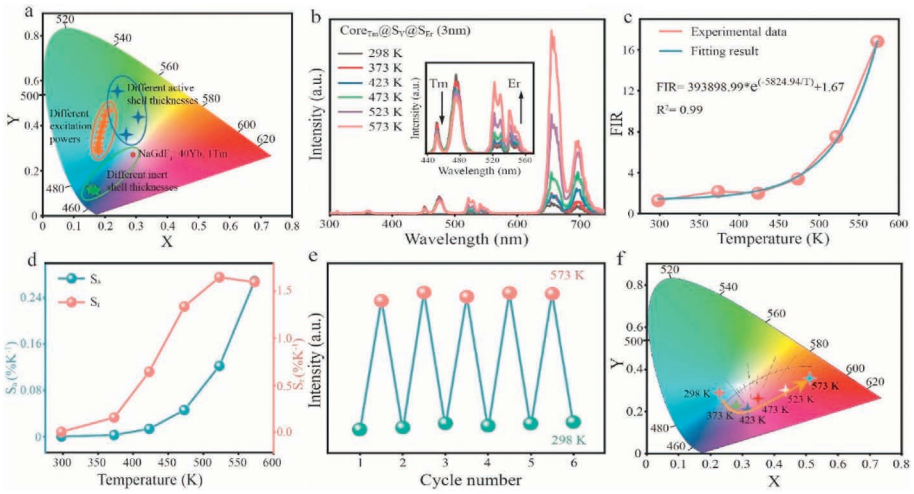


Fig. 3. Upconversion luminescence color modulation and temperature measurement performance. (a) Summary of CIE under different treatment conditions. (b) Temperature-dependent luminescence spectra of Core$_{Tm}$@S$_Y$@S$_{Er}$ with an active shell layer thickness of 3 nm under 980 nm laser excitation. (c) Plots of experimentally measured and exponentially fitted values of the luminescence intensity ratio of Core$_{Tm}$@S$_Y$@S$_{Er}$ at 475 nm and 655 nm at different temperatures. (d) Calculated S_a and S_r *versus* temperature based on the Core$_{Tm}$@S$_Y$@S$_{Er}$ UCNPs. (e) Temperature-dependent upconversion luminescence intensity variation of Core$_{Tm}$@S$_Y$@S$_{Er}$ over five cycles at 655 nm. (f) Color coordinates of Core$_{Tm}$@S$_Y$@S$_{Er}$ as a function of temperature.

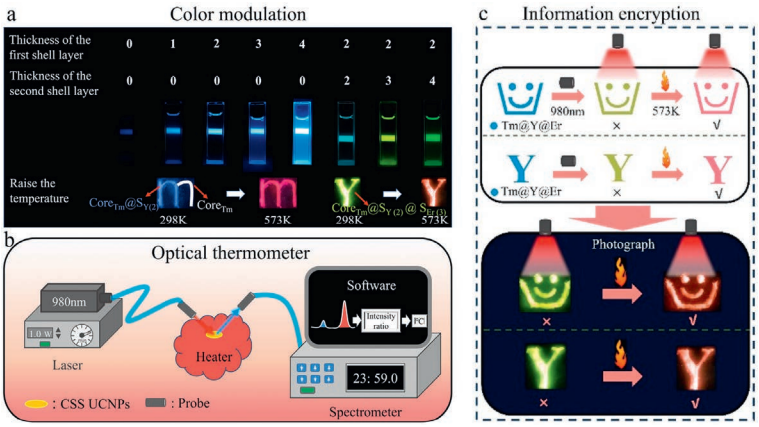


Fig. 4. Luminescent application extension. (a) Color modulation by changing the thickness of the shell layer. The number represents the thickness of the corresponding shell layer. (b) Schematic of Core$_{Tm}$@S$_Y$@S$_{Er}$ UCNPs being applied to temperature sensing. (c) Schematic of the information encryption. Codes in red indicate correct information, the rest are errors.

UCNPs offered great advantages for applications such as display and information security in harsh environments.

More interestingly, the unique encapsulable structure and thermo-responsive properties of the nanoparticles enabled the achievement of highly saturated RGB colors, tunable emission, and a wide color gamut. This can be realized by adjusting the shell thickness, incorporating additional activators, and modulating the ambient temperature (Fig. 4a). The fast thermal response, high thermal stability, and apparent temperature-dependent behavior of luminescent colors of Core$_{Tm}$@S$_Y$@S$_{Er}$ UCNPs provided new opportunities for cutting-edge applications in temperature detection and information encryption. Utilizing the thermo-responsive properties of the UCNPs described above, a conception for detecting the surface temperature of a high-temperature object was provided. Core$_{Tm}$@S$_Y$@S$_{Er}$ UCNPs were fabricated into uniformly distributed thin films and immobilized on the surface of a high-temperature object. The intensity of the blue and red emission bands under 980 nm excitation was then monitored by a spectrometer and compared with a predetermined reference value to derive the current actual temperature of the object. If only an approximate surface temperature was desired, the tester can observe the color by shining a laser directly on it (Fig. 4b). As an additional benefit, the luminescent color of the nanomaterials gradually changed from green to red during the heating process (Fig. 4c), providing an ideal candidate for information security and anti-counterfeiting applications. For the "smiley face and letter" design, it only displayed a green "smiley face and Y" icon under 980 nm excitation, whereas it turned into a red "smiley face and Y" icon when the background temperature was increased to 573 K. This combination of photothermal triggers has the unique advantage of being reusable and extremely high-resolution (Fig. S20 in Supporting information).

In summary, the novel design of Core$_{Tm}$@S$_Y$@S$_{Er}$ UCNPs was demonstrated here, which has certain advantages in the fields of upconversion luminescence color control, temperature sensing and information encryption. The photoluminescence spectrum and the precise control of the shell thickness revealed that the more the inert shell was coated, the better the luminescence performance in the blue region. By exploiting the relationship between the active shell and the core to compete for near-infrared photon energy, the luminescence color of the whole UCNPs can be effectively controlled from blue to green. In addition, the thermal quenching behavior of Tm and the negative thermal quenching behavior of Er can occur simultaneously through the design of Core$_{Tm}$@S$_Y$@S$_{Er}$ structure. What's more, this thermally correlated special lumines-

cence behavior achieved a relative sensitivity of 1.64 %/K and an absolute sensitivity of 0.26 %/K, providing valuable experience for the fabrication of ultra-high-performance temperature probes. Finally, the color gamut span of the luminescent color from light green to red as the temperature increases confirmed its potential for application in communication encryption and security.

Declaration of competing interest

The authors declare that they have no known competing financial interests or personal relationships that could have appeared to influence the work reported in this paper.

CRediT authorship contribution statement

Bingyu Huang: Writing – original draft, Methodology, Investigation, Formal analysis, Data curation. **Jipeng Fu:** Writing – review & editing, Supervision, Methodology, Investigation, Funding acquisition, Formal analysis. **Tianyi Sun:** Writing – original draft, Formal analysis, Data curation. **Yuqi Li:** Formal analysis, Data curation. **Jinru Liu:** Formal analysis, Data curation. **Kaina Wang:** Methodology, Investigation, Formal analysis. **Qian Xu:** Methodology, Investigation, Data curation. **Wengui Yu:** Software, Methodology, Data curation. **Hongqi Chen:** Methodology. **Huajie Luo:** Software, Investigation, Data curation. **Mathieu Allix:** Writing – review & editing, Formal analysis. **Mingxue Tang:** Writing – review & editing, Formal analysis. **Shiqing Xu:** Funding acquisition, Formal analysis.

Acknowledgments

This work was supported by the National Natural Science Foundation of China (No. 62205322); the China Postdoctoral Science Foundation funded project (No. 2023M733157); and the Fundamental Research Funds for the Provincial Universities of Zhejiang (No. 2021YW46); the fund of Key Laboratory of Advanced Materials of Yunnan Province (No. 2024KF03); the Key Research and Development Project in Zhejiang Province (No. 2022C01133). The computational resource was provided by the Center for High Pressure Science and Technology Advanced Research.

Supplementary materials

Supplementary material associated with this article can be found, in the online version, at doi:10.1016/j.cclet.2025.111159.

References

[1] S.K. Ling, Y.X. Wang, X.Y. Qin, et al., Inorg. Chem. 63 (2024) 6660–6673.
[2] J.S. Liao, M.H. Wang, F.L. Lin, et al., Nat. Commun. 13 (2022) 2090.
[3] B.Z. Zheng, D.N. Zhong, T.T. Xie, et al., Chem 7 (2021) 1615–1625.
[4] K.N. Wang, J.P. Fu, H.L. Dong, et al., Small Struct. 5 (2024) 2400092.
[5] D. Li, M.C. Jia, T. Jia, G.Y. Chen, Adv. Mater. 36 (2024) 2309452.
[6] Y. Hong, Y.Q. Jiang, C.H. Yuan, et al., Chin. Chem. Lett. 35 (2024) 109909.
[7] Z.Q. Ge, Z.X. Pan, Yan S, et al., Chin. Chem. Lett. 35 (2024) 109850.
[8] J.J. Zhou, B.D. Rosal, D. Jaque, S. Uchiyama, D.Y. Jin, Nat. Methods 17 (2020) 967–980.
[9] S.Y. Han, R.R. Deng, Q.F. Gu, et al., Nature 587 (2020) 594–599.
[10] K. Malhotra, D. Hrovat, B. Kumar, et al., ACS Appl. Mater. Interfaces 15 (2023) 2499–2528.
[11] Y.L. Chang, H.R. Chen, X.Y. Xie, et al., Nat. Commun. 14 (2023) 1079.
[12] J.P. Fu, R. Pang, L.H. Jiang, et al., Dalton Trans. 45 (2016) 13317–13323.
[13] C.D.S. Brites, R. Marin, M. Suta, et al., Adv. Mater. 35 (2023) 2302749.
[14] M. Yang, H.J. Gong, D. Yang, et al., Chin. Chem. Lett. 35 (2024) 108468.
[15] Q.Q. Li, X.Y. Xie, H. Wu, et al., Nano Lett. 23 (2023) 3444–3450.
[16] K. Trejgis, K. Ledwa, K. Maciejewska, L. Li, L. Marciniak, Sci. Rep. 12 (2022) 5847.
[17] Y. Xue, Y.Q. Chen, G.X. Li, et al., Chin. Chem. Lett. 35 (2024) 108447.
[18] M. Liu, J.Y. Liang, F. Vetrone, Acc. Chem. Res. 57 (2024) 2653–2664.
[19] X. Qu, P.Z. Wu, K.X. Duan, et al., Chin. Chem. Lett. 35 (2024) 109681.
[20] Y.B. Wang, L. Lei, G.Ye R, et al., ACS Appl. Mater. Interfaces 13 (2021) 23951–23959.
[21] C. Mi, J.J. Zhou, F. Wang, G.G. Lin, D.Y. Jin, Chem. Mater. 31 (2019) 9480–9487.
[22] S.Y. Han, Z.G. Yi, J.B. Zhang, et al., Nat. Commun. 12 (2021) 3704.
[23] H. Xu, S.Y. Han, R.R. Deng, et al., Nat. Photon. 15 (2021) 732–737.
[24] B.Z. Zheng, J.Y. Fan, B. Chen, et al., Chem. Rev. 122 (2022) 5519–5603.
[25] S.Q. Chang, J.P. Fu, X. Sun, et al., Inorg. Chem. 61 (2022) 3746–3753.
[26] F. Li, L.P. Tu, Y.Q. Zhang, et al., Nat. Photonics 18 (2024) 440–449.
[27] K.N. Wang, J.P. Fu, S.B. Zhan, et al., Chem 11 (2025) 102325.
[28] K.N. Wang, J.P. Fu, S.Q. Chang, et al., Adv. Powder Mater. 2 (2023) 100112.
[29] Y.H. Wang, Z.C. An, Z.R. Tao, et al., J. Phys. Chem. Lett. 13 (2022) 12032–12040.
[30] Y.L. Wang, J.H. Rui, H. Song, et al., J. Am. Chem. Soc. 146 (2024) 6530–6535.
[31] H.M. Liu, L. Yan, J.S. Huang, et al., J. Phys. Chem. Lett. 13 (2022) 2306–2312.
[32] L. Marciniak, W. Piotrowski, M. Szalkowski, et al., Chem. Eng. J. 427 (2022) 131941.
[33] X.F. Wu, S.P. Zhan, J.B. Han, Y.X. Liu, Nano Lett. 21 (2021) 272–278.
[34] W.Q. Cao, Z.L. Liao, H.X. Chen, et al., ACS Appl. Mater. Interfaces 16 (2024) 58920–58930.
[35] Z.H. Chen, Y.K. Cun, S.L. Yan, et al., Sci. China Mater. 66 (2023) 4742–4748.
[36] Y.Z. Zi, Z.W. Yang, Z. Xu, et al., J. Alloys Compd. 880 (2021) 160156.
[37] E.D. Martínez, C.D.S. Brites, L.D. Carlos, et al., Adv. Funct. Mater. 29 (2019) 1807758.
[38] J.J. Zhou, S.H. Wen, J.Y. Liao, et al., Nat. Photonics 12 (2018) 154–158.
[39] J.S. Huang, L. Yan, C.An Z, et al., Adv. Mater. 36 (2024) 2310524.
[40] X. Sun, W. Dong, C.J. Lou, et al., J. Solid State Chem. 316 (2022) 123640.
[41] Z.C. An, Q.Q. Li, J.S. Huang, L.L. Tao, B. Zhou, Nano Lett. 23 (2023) 6241–6248.
[42] H.H. Fu, C.H. Hu, J. Liu, et al., CrystEngComm 24 (2022) 7698–7717.
[43] J.Y. Chen, L.L. Liang, S.D. Tan, et al., Nano Lett. 23 (2023) 7221–7227.
[44] R. Shi, C.D.S. Brites, L.D. Carlos, Small Struct. 3 (2022) 2100194.
[45] Y. Wang, J.X. Low, Y.F. Bi, et al., Chin. Chem. Lett. 33 (2022) 1087–1090.
[46] H.Y. Xu, M.C. Jia, Z.Y. Wang, Y.L. Wei, Z. L. Fu, ACS Appl. Mater. Interfaces 13 (2021) 61506–61517.
[47] L. Yan, J.S. Huang, Z.C. An, Q.Y. Zhang, B. Zhou, Nano Lett. 22 (2022) 7042–7048.
[48] Q.L. Zou, C. Marcelot, N. Ratel-Ramond, et al., ACS Nano 16 (2022) 12107–12117.
[49] Y. Zhang, P.P. Lei, X.H. Zhu, Y. Zhang, Nat. Commun. 12 (2021) 6178.
[50] Y.H. Wei, S. Yang, K.H. Zhu, et al., Laser Photon. Rev. 18 (2024) 2400612.
[51] J.W. Jin, J. Lin, Y.P. Huang, et al., Chin. Chem. Lett. 33 (2022) 4798–4802.